A generalised geometrical model of turning operations for cutting force modelling using edge discretisation

S. Campocasso[a,*], J.-P. Costes[a], G. Fromentin[a], S. Bissey-Breton[b], G. Poulachon[a]

[a] *Arts et Metiers ParisTech, LaBoMaP, Rue Porte de Paris, 71250 Cluny, France*
[b] *CEA, DAM, Valduc, 21120 Is-sur-Tille, France*

Abstract

The knowledge of cutting forces is of prime importance to ensure the success of cutting operations, the desired properties of the machined parts and therefore the functionality of the workpieces.
Edge discretisation is one way to model cutting forces. Traditionally used in milling, this methodology enables local changes in uncut chip thickness or cutting geometry to be taken into account and then gives suitable results in the three directions. A key point of this method is the geometrical transformation that enables the description of various tool geometries.
This study proposes a geometrical model based on homogeneous matrices, whose main interest is to decompose the transformations step-by-step. The method, generalisable to all machining operations, is detailed for turning operations. Inserted cutters are modelled considering both the positioning of the insert and the local geometry of the insert.
The cutting geometry and the edge are described using the same model in the machine coordinates system, allowing forces and moments to be calculated easily.

Keywords: Cutting force modelling, Edge discretisation, Tool geometry, Homogeneous matrix transformations, Turning operations

Nomenclature

α_{ne}	Working normal clearance angle; defined in P_n [1]
α_n^P	Normal clearance angle given by the local preparation (P) of the insert; defined in P_n
α_{oe}	Working orthogonal clearance angle; defined in P_{oe} [1]
γ_{ne}	Working normal rake angle; defined in P_n [1]
γ_n^P	Normal rake angle given by the local preparation (P) of the insert; defined in P_n
ε^E	Tool included angle of the cutting edge (E); also denoted ε_r if the cutting edge is included in P_r [1]
η	Chip flow angle
θ	Polar angle defined in a coordinate system linked to the insert (parameterisation of the cutting edge)
Θ	Polar angle defined in a coordinate system linked to the machine ($\Theta = \theta + \kappa_r + \varepsilon_r/2 - \pi/2$)
κ_r'	Tool minor cutting edge angle; defined in P_r [1]
κ_r^B	Tool cutting edge angle of the major cutting edge during cylindrical turning (or κ_r [1])
κ_{re}	Working cutting edge angle; defined in P_{re} [1]
λ_{se}	Working cutting edge inclination angle; defined in P_{se} [1]
λ^E	Inclination angle given by the local curvature of the cutting edge (E)
ψ_f^B	Tilting angle defining the positioning of the insert on the tool body (B); defined in P_f
ψ_p^B	Tilting angle defining the positioning of the insert on the tool body (B); defined in P_p
A_D	Nominal cross-sectional area of the cut [2]
a_p	Depth of cut (Back engagement of the cutting edge [2])
f	Feed [2]
$\overrightarrow{f}$	Local linear forces
$\overrightarrow{F_x}$	Global force applied to the tool in the machine X axis direction (idem for F_y and F_z)

*Corresponding author. Tel.: +33 385595388.
Email addresses: sebastien.campocasso@ensam.eu (S. Campocasso), jean-philippe.costes@ensam.eu (J.-P. Costes), guillaume.fromentin@ensam.eu (G. Fromentin), stephanie.breton@cea.fr (S. Bissey-Breton), gerard.poulachon@ensam.eu (G. Poulachon)

h Local thickness of cut [2]
h_{max} Maximum uncut chip thickness on the active cutting edge
K_c Specific cutting force
L_S Length of the considered segment
M Current point on the cutting edge
$\mathcal{M}_{x,C}$ Moment around $\vec{X_M}$ at point C
N_{Seg} Number of segments used in the discretisation
P_f Assumed working plane [1]
P_n Cutting edge normal plane [1]
P_{oe} Working orthogonal plane [1]
P_p Tool back plane [1]
P_r Tool reference plane [1]
P_{re} Working reference plane [1]
P_{se} Working cutting edge plane [1]
r_β Rounded cutting edge radius (standardised notation: r_n [1])
r_ε^E Corner/nose radius; also denoted r_ε if the cutting edge is included in P_r [1]
R^E Polar radius (parameterisation of the cutting edge)
R_o^W Radius of the workpiece (W) in the plane P_o
$\overrightarrow{v_c}$ Local cutting speed [1]
$\overrightarrow{v_e}$ Local resultant cutting speed [1]
$\overrightarrow{V_f}$ Feed speed [1]
x^M Machine axis translation in the X direction (defined by [3])
z^M Machine axis translation in the Z direction (defined by [3])

1. Introduction

The modelling of cutting forces is essential to predict the progress of machining operations as well as the final properties of workpieces. At a large scale, the cutting forces can be used to size the clamping system [4] or to predict the deflections [5] or the vibrations [6–11] of the tool, the part or the structure, in order to ensure the geometry and the roughness characteristics of the machined surface. When focusing on the tool-part interface, numerous studies have tried to link cutting forces to residual stresses [12] or surface integrity, and then predict fatigue life or corrosion resistance [13].

More and more manufacturers wish to adapt the cutting parameters in order to obtain the expected properties of the workpiece. For example, the feed can be modified along the tool path in order to limit the cutting forces, while minimising the cycle time [14, 15]; the machining allowance may also be variable. The feed can be adapted in real-time by measuring the forces and modifying the numerical command (NC) instructions [16]. Nevertheless, predictive methods should be preferred because of the cost of the monitoring equipment and the difficulties in modifying the NC command data or the set-point value in the speed control loop. Moreover, simply respecting a maximum force does not ensure the smooth progress of the cutting process. As a consequence, there is a need for cutting force models which can be used for complex and various cutting operations.

In a literature review conducted in 1998 [17], the authors noted that cutting force models are too rarely used in industry, because they are not well formalised and the validity domain is not clearly specified.

The aim of the present study is to propose a methodology which enables the description of cutting operations when turning with inserted tools.

A brief review of cutting force modelling by mechanistic approaches is first proposed. Then a geometrical model using homogeneous matrix transformations is presented. Next, the cutting geometry is described and the main factors affecting the forces are calculated in order to be used as inputs for the cutting force models. Finally, the forces and moments applied to the tool can be calculated.

In this article, most notations used are consistent with ISO standards [1–3]. The notations $\overrightarrow{F_x}$, $\overrightarrow{F_y}$ and $\overrightarrow{F_z}$ correspond respectively to the radial, tangential and axial components of the global forces (in Newtons). The local forces (in N/mm) are denoted with a lowercase $\overrightarrow{f}$.

2. Mechanistic modelling and edge discretisation - A state of the art

2.1. Origin of the mechanistic models

As the physical modelling of the cutting process is complex, due to the number of uncertain local parameters, mechanistic models, which are easier to handle, have been developed. The form of the cutting relations is

elaborated starting from the observation of the mechanical effects of the machining parameters. Then the model is identified from a set of tests, which limits the validity domain [9].

Mechanistic models involve the operative parameters, as well as the tool and workpiece geometries, from which other parameters, like the chip load, are calculated [18].

Classically, the chip load is considered as the nominal cross-sectional area of the cut A_D, which is linked to the cutting force by the specific cutting force K_c. Therefore, when contour turning is considered, many elementary areas should be calculated and a macroscopic chip flow direction is required to estimate the axial and radial components [6, 19].

Some authors try to link the operative cutting parameters f (feed) and a_p (depth of cut) directly to the cutting forces [20]. However, sometimes these parameters have no physical sense, especially when only the nose of the tool is cutting. This is why approaches like ANOVA or RSM (Response Surface Methodology) generally conclude that the interaction between these two parameters is non negligible; the link is geometric and corresponds to the local undeformed chip thickness h.

Thus a geometric analysis can be helpful to determine the local cutting conditions, which are more representative of the cutting process.

This considered, if a global approach is nevertheless preferred, an effective or mean uncut chip thickness [21, 22] or the maximum uncut chip thickness h_{max} [23] may be used.

2.2. Edge discretisation methodology

In the early 1960's, Sabberwal [24] showed that the cutting force is proportional to the width of cut in flank milling.

This observation allows us to consider that the cutting forces applied to the tool are the sum of the local contributions. The active cutting edge is then generally discretised into segments and the tool is considered as a sum of elementary rectilinear edged tools.

It should be noted that the assumption of the independence of the elementary tools is implicit; consequently, the curvatures of the edge and the rake face are neglected [25].

The edge discretisation methodology was originally used to consider the temporal slippage of edge elements when flank milling [24, 26] and has been taken up in many studies.

In turning, this methodology enables the local value of the uncut chip thickness to be taken into account when round-nosed tools are used [27].

Shaw et al. [28] began to analyse the variation in cutting geometry along a cutting edge and the possible effects on the cutting forces. Later, one of the first applications of the edge discretisation method to take the local geometry into account was proposed by Armarego and Cheng [25] for drilling operations.

The edge discretisation method can be used with analytical or numerical local cutting models, representative of orthogonal or oblique cutting operations. However, mechanistic models are the most widely used due to their simplicity.

2.3. Local cutting models

A local cutting model is defined by the cutting relations linking the local forces to the parameters (scalar relationships) and also by the basis in which the local forces are expressed. Various local bases can be used; the most common are presented in this paragraph.

In milling, three forces are classically defined in the Radial-Tangential-Axial (RTA) basis [29]. When considering ball-end mills, this basis is normal to the sphere-envelope [30] and the RTA denomination is not proper; it is also the case whenever κ_r is not equal to 90°, as for turning operations.

Bissey et al. [31] propose to use the local basis denoted ($\overrightarrow{o}$, $\overrightarrow{v}$, $\overrightarrow{h}$) and defined as follows: $\overrightarrow{v}$ is parallel to the cutting speed $\overrightarrow{V_c}$, $\overrightarrow{h}$ is the intersection between the reference plane P_r and the cutting edge normal plane P_n (measurement direction of h) and $\overrightarrow{o}$ completes the basis. This basis can be qualified as semi-global, because it is oriented both by the tool (cutting edge angle κ_r taken into account) and by the machine (primary motion).

One of the most popular local cutting models was proposed by Thaulow in 1942 - as reported in the discussion in reference [32] - and considers that the forces are expressed with an affine relation with respect to h. This law is explainable by observing the results of orthogonal cutting tests [33] when h is large compared to the edge radius r_β.

Accordingly, the three components $\overrightarrow{f_v}, \overrightarrow{f_h}, \overrightarrow{f_o}$ (Fig. 1 (a)) are expressed with an affine relation (Eq. (1)) [29]. If there is no inclination, component f_o is equal to zero.

$$f_i = K_{ci}\, h + k_{ei} \quad \text{with} \quad i = o, v, h \tag{1}$$

Coefficients K_{ci} represent the chip load contribution, while k_{ei} corresponds to the edge effect [34]. As the cutting angles do not appear in this model, the four identified coefficients are only available for one type of local cutting geometry (edge preparation).

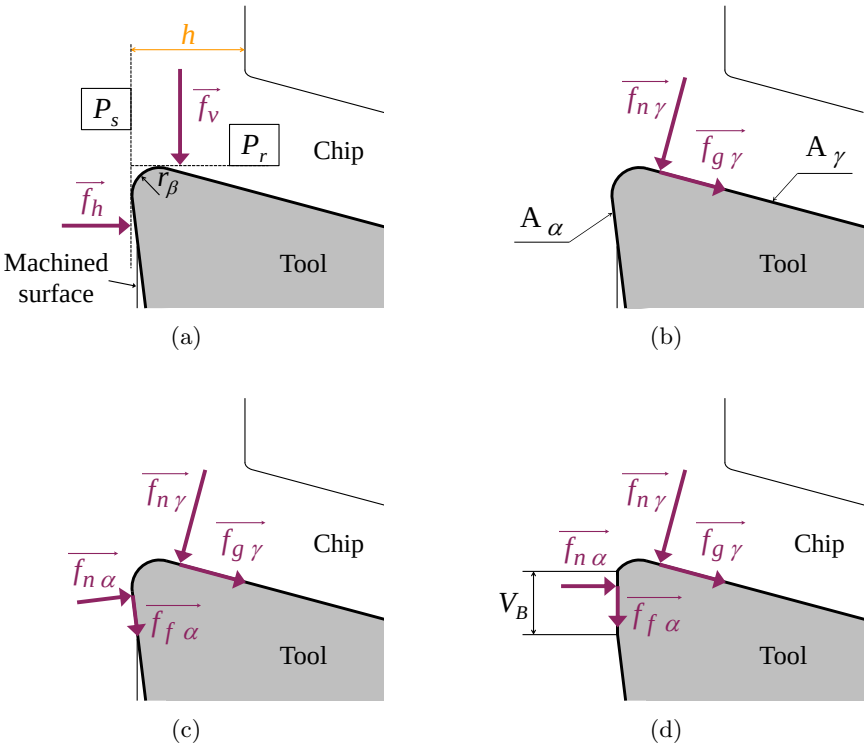

Figure 1: Possible applications of the local forces: (a) in the $(\vec{o}, \vec{v}, \vec{h})$ basis; (b) on the rake face; (c) on the rake and clearance faces; (d) on the worn clearance surface (or the rounded edge).

In order to enhance the physical meaning, it is possible to apply the local forces on the rake face $\mathcal{A}_\gamma$ as shown in Fig. 1 (b) [35, 36]. In this case, the force $\overrightarrow{f_{n\gamma}}$ is applied normal to the rake face and the tangential force $\overrightarrow{f_{g\gamma}}$ - or $\overrightarrow{f_{f\gamma}}$ if oriented by a chip flow angle - represents the friction.

To take into account the clearance contact (Fig. 1 (c)), local forces can be also applied on the rake and clearance faces $(\overrightarrow{f_{n\alpha}}, \overrightarrow{f_{g\alpha}})$ [37, 38].

Some authors replace the clearance face $\mathcal{A}_\alpha$ with the surface created by flank wear, which brings back the forces normally applied to $\mathcal{A}_\alpha$ in the $(\overrightarrow{o}, \overrightarrow{v}, \overrightarrow{h})$ basis (Fig. 1 (d)) [12]. The same result is obtained by authors who consider that the tool/workpiece contact is localised in the rounded edge [39].

2.4. Generalisation of the cutting force models

In 1985, the structure of a unified multi-operations model, shown in Fig. 2, was set out by Armarego and Whitfield [34] and has been completed since then [40]. Cutting relations are established in orthogonal or oblique cutting and a database of identified coefficients is constituted from the results of elementary cutting tests conducted on various materials. Cutting relations and identified coefficients are available for a given edge preparation / machined material pair; chip breakers should also be fixed.

At the heart of this approach is the interface between the oblique analysis and the applications, which consists of geometrical transformations. The simpler these transformations are, the more industrial applications can be expected for them.

In the next section, a mathematical interface between the cutting model and the applications, built on homogeneous matrix transformations, is presented. This methodology is a generalisation and an improvement of a previous work concerning round inserts [38]. The application of the present paper is limited to 2-axis turning with inserted tools, but the method can be applied to any machining operation.

As indicated by Kaymakci et al. [36], geometrical modelling is independent of the local cutting model used to calculate the forces. For this reason, cutting models are not discussed further in this paper.

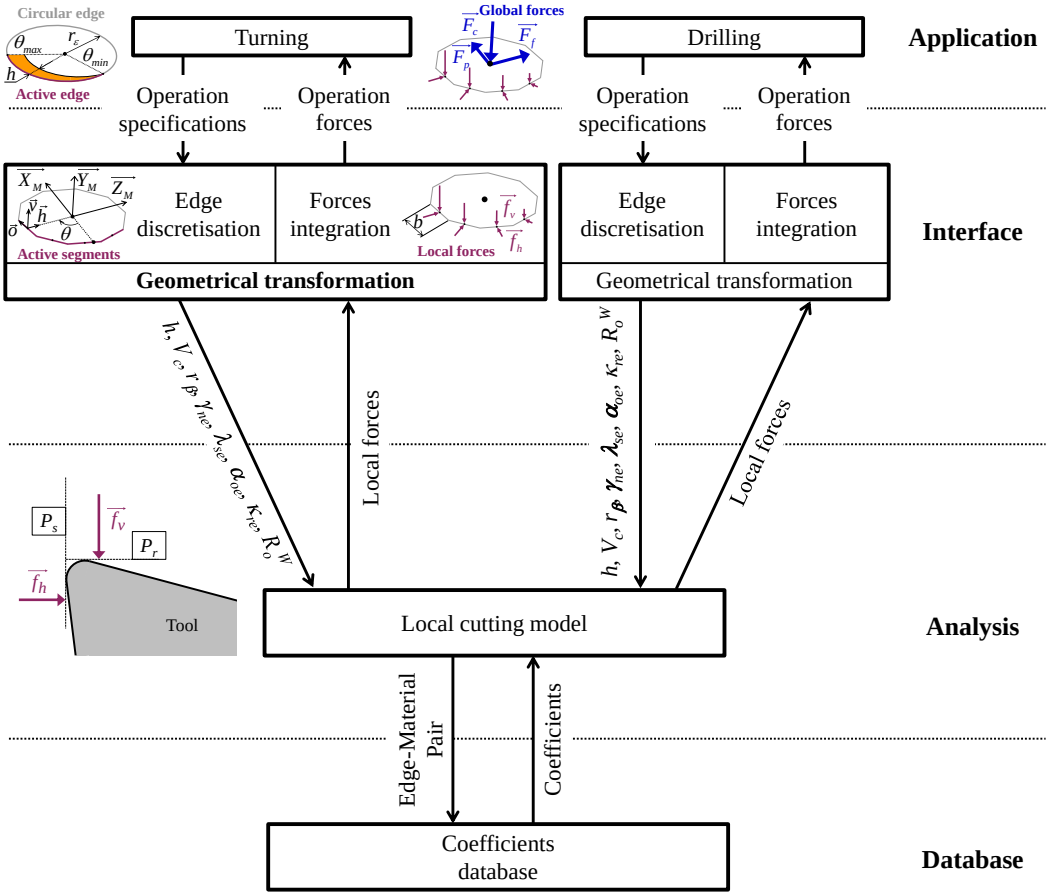

Figure 2: Principle of a multi-operation cutting force model (adapted from [34]).

3. Geometrical modelling of turning operations

3.1. General principle of geometrical modelling

The calculation of cutting forces by edge discretisation requires the knowledge of several geometrical parameters.

The most significant parameters are the uncut chip thickness h and the rake angle γ_n, while the effect of the cutting speed V_c is often not significant [20]. These parameters can be used in expressions of the local forces, such as the inclination angle λ_s which is also often taken into account [35]. The clearance angle and the edge radius r_β are rarely considered, but they could be introduced. Recent work suggests that the cutting edge angle κ_r and the radius of curvature of the workpiece R_o^W should also be taken into account [41].

In order to calculate the uncut chip thickness, it is helpful to have a definition of the cutting edge in a coordinate system linked to the workpiece.

Concerning the calculation of the working cutting angles, the tool geometry should be expressed in a basis given by the cutting and feed movements.

In addition, to be compared with measured forces, the calculated forces must be expressed in the same basis as that of the measured ones.

In the particular case of turning, these three bases are coincident.

The principle of the method, summarised in Fig. 3, is that any cutting operation with inserted cutters can be modelled by considering each of the following transformations:

- the joint movements of the machine (translations and rotations, if any), represented by the matrix $\mathcal{M}_{Machine}$ and given by the trajectory and, in some cases, the orientation of the tool;
- the positioning of the insert on the tool body: $\mathcal{M}_{Body}$;
- the shape of the cutting edge (global shape of the insert): $\mathcal{M}_{Edge}$;
- the local cutting geometry of the insert (edge preparation): $\mathcal{M}_\gamma$ and $\mathcal{M}_\alpha$ respectively for the rake and clearance faces.

The notations for angles and distances used in the transformations are the following: κ_r^B means that the angle is given by the element B (for Body) and considered in the plane P_r.

The planes and their reference systems are defined by the ISO 3002-1 standard [1].

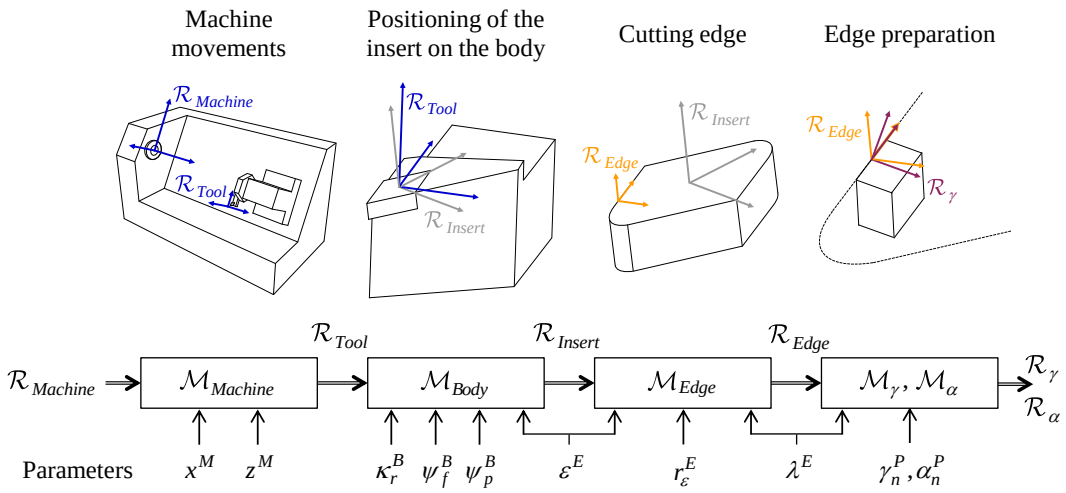

Figure 3: Graphic summary of the method, illustrated for turning.

3.2. Principle of modelling by homogeneous matrix transformations

The use of rotation matrices is the common way to transform a local basis into the measurement basis [6, 7, 11, 21, 37], even in orthogonal cutting [39].

The limit of the 3x3 matrix transformations is that the cutting edge should be described by a stand-alone representation [7, 21, 37].

Since Denavit and Hartenberg [42] introduced homogeneous matrices, they have commonly been used for the kinematical description of machine-tools, particularly for 5-axis milling centers [43].

Later, the cutting geometry obtained from grinding kinematics were modelled by homogeneous transformations [44].

Rivière-Lorphèvre [9] note that these transformations can also be used to describe cutting operations in order to model cutting forces, as do Sambhav et al. [45].

The interest of homogeneous transformations is to consider local coordinate systems, rather than vector bases, which enables the edge and the local geometry to be described simultaneously. In turning, the coordinate systems linked to the dynamometer, the workpiece and the motions are the same, and correspond to that linked to the machine, denoted $\mathcal{R}_{Machine} = (\overrightarrow{X_M}, \overrightarrow{Y_M}, \overrightarrow{Z_M}, O_{Pr})$. O_{Pr} corresponds to the origin of the NC program (on the spindle axis).

3.3. Parameterisation of the machine (M) movements - Tool trajectory

The conventions for axis definition are given by the ISO 841 standard [3]. All the presented applications are performed for a rear turret lathe.

As previously mentioned, the use of homogeneous matrices for the description of machine axis movements is common when a 5-axis machine is considered. In 2-axis turning, the first matrix of the model involves only the two translations x^M and z^M. If cutter radius compensation (CRC) is used, the matrix is simply written under Eq. (2) for the k^{th} spindle revolution. This matrix represents the trajectory of the nose centre, denoted C_ε (Fig. 4).

$$\mathcal{M}_{Machine}(k) = \begin{pmatrix} 1 & 0 & 0 & x^M(k) \\ 0 & 1 & 0 & 0 \\ 0 & 0 & 1 & z^M(k) \\ 0 & 0 & 0 & 1 \end{pmatrix} \tag{2}$$

If CRC is not used in the NC program, the value of the corner radius r_ε must be added to consider the nose centre instead of the cutter reference (point P).

3.4. Parameterisation of the positioning of the insert on the tool body (B)

Unfortunately, the ISO 3002 standard [1] is not well adapted to inserted tools. Indeed, this standard refers to HSS tools, and the positioning of inserts is not considered.

Thus, the positioning of the insert on the cutter body is defined by three angles: the cutting edge angle κ_r^B defined in P_r [1], and two tilting angles (Fig. 5), whose definition is not clear. The first one, κ_r^B, is defined between the major cutting edge and the feed direction for cylindrical turning. The two last angles are defined

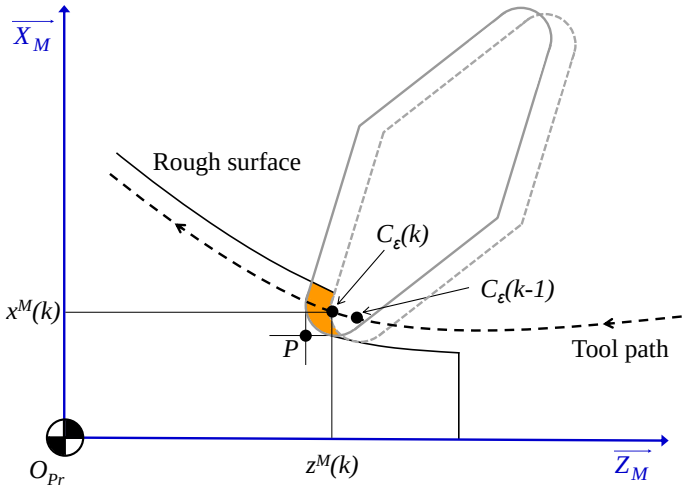

Figure 4: Machine axis and tool trajectory.

by tool manufacturers around $\overrightarrow{X_M}$ and $\overrightarrow{Z_M}$ and can be respectively called rake angle γ^B and inclination angle λ^B [38, 46, 47], or axial rake angle γ_f^B (in P_f) and radial rake angle γ_p^B (in P_p) [7, 36]. It should be noted that the denomination axial/radial rake angles enables us to draw a parallel with milling operations, but the conventions must be redefined: in flank milling, γ_f^B is the radial rake angle and γ_p^B is the axial rake angle.

As these angles simultaneously modify all the working angles γ_{ne}, α_{ne} and λ_{se} along the cutting edge, the denomination "rake angles" does not seem appropriate. In this paper, these tilting angles are denoted:

- ψ_f^B for the tilt in P_f;
- ψ_p^B for the tilt in P_p.

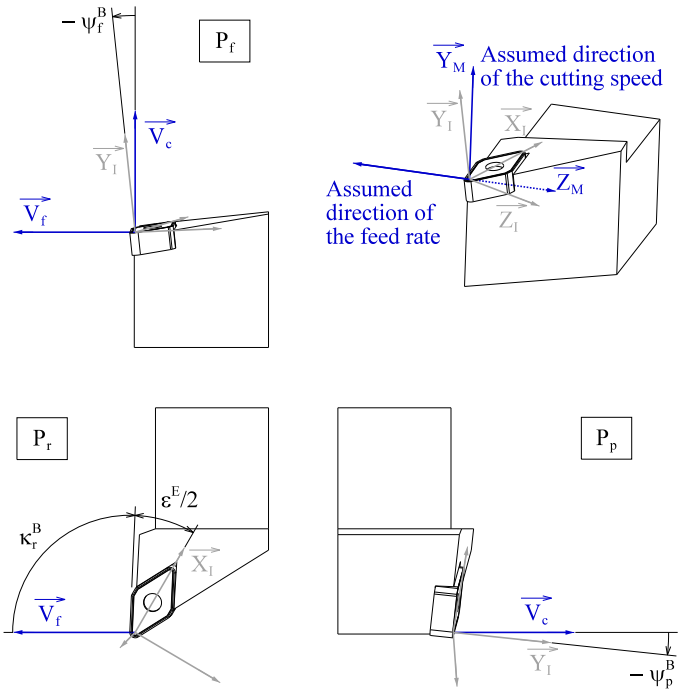

Figure 5: Positioning of the insert on the tool body: cutting edge angle κ_r^B and tilting angles ψ_f^B and ψ_p^B (see also [36]).

In order to be extended to rotating tools (milling cutters, drills), the method should consider the rotation and the run-out at this level, and of course the different teeth of the tool.

3.4.1. Matrix composition

Classically, the rotation of the insert is obtained by multiplying three rotation matrices [7, 21, 36, 38]. However, matrix multiplication is not commutative and the three angles are defined from the same basis (P_r, P_f and P_p are orthogonal). Thus, since the result of the matrix calculation depends on the chosen sequence of

rotations, the problem cannot be rigorously modelled by matrix compositions.

While error is negligible for tilting angles ψ_f^B and ψ_p^B due to their low value (between 0 and $-10\,^\circ$), it becomes a problem when κ_r^B is considered because of its higher variations.

There is therefore a need for a method to express a specific matrix describing the positioning of the insert.

3.4.2. SORA Method

The Simultaneous Orthogonal Rotations Angle (SORA) method, proposed by Tomažic and Stančin [48] in the field of electrical engineering, could lead to a solution to this problem.

The simultaneous rotations are written in the form of a vector, called SORA vector and denoted here $\underline{\mathcal{V}}_{Body}$. This vector is expressed in the machine coordinate system (or $\mathcal{R}_{Tool}$) by Eq. (3).

$$\underline{\mathcal{V}}_{Body} = \begin{bmatrix} \psi_f^B \\ \\ \dfrac{\pi}{2} - \kappa_r^B - \dfrac{\varepsilon^E}{2} \\ \\ -\psi_p^B \end{bmatrix}_{\mathcal{R}_{Tool}} \tag{3}$$

The rotation vector $\underline{\mathcal{V}}_{Body}$ corresponds to a single rotation, whose angle (modulus) ϕ^B and orientation $\overrightarrow{v}^B$ can be calculated by Eq. (4) and (5).

$$\phi^B = ||\underline{\mathcal{V}}_{Body}|| \tag{4}$$

$$\overrightarrow{v}^B = \begin{bmatrix} v_x \\ v_y \\ v_z \end{bmatrix} = \frac{\underline{\mathcal{V}}_{Body}}{\phi^B} \quad \text{if} \quad \phi^B \neq 0 \tag{5}$$

Finally, a homogeneous matrix $\mathcal{M}_{Body}$, representing the positioning of the tool insert on the body, can be calculated according to Rodrigues' rotation formula (Eq. (6)).

$$\begin{aligned} \mathcal{M}_{Body} = \cos\phi^B \begin{pmatrix} 1 & 0 & 0 & 0 \\ 0 & 1 & 0 & 0 \\ 0 & 0 & 1 & 0 \\ 0 & 0 & 0 & M_{44} \end{pmatrix} + (1-\cos\phi^B) \begin{pmatrix} v_x^2 & v_xv_y & v_xv_z & 0 \\ v_xv_y & v_y^2 & v_yv_z & 0 \\ v_xv_z & v_yv_z & v_z^2 & 0 \\ 0 & 0 & 0 & M_{44} \end{pmatrix} \\ + \sin\phi^B \begin{pmatrix} 0 & -v_z & v_y & 0 \\ v_z & 0 & -v_x & 0 \\ -v_y & v_x & 0 & 0 \\ 0 & 0 & 0 & M_{44} \end{pmatrix} \quad \text{with} \quad M_{44} = \frac{1}{1+\sin\phi^B} \end{aligned} \tag{6}$$

To consider round inserts, the cutting edge angle κ_r^B and the tool included angle ε^E must be taken as respectively equal to $\pi/2$ and 0.

The matrix $\mathcal{M}_{Body}$ enables the transformation of $\mathcal{R}_{Tool}$ into the coordinate system $\mathcal{R}_{Insert} = (\overrightarrow{X_I}, \overrightarrow{Y_I}, \overrightarrow{Z_I}, C_\varepsilon)$ linked to the insert, whose X axis corresponds to the bisectrix of the insert.

The results obtained for two different composition sequences (cf. Section 3.4.1) and the SORA method are compared in Fig. 6 for a circular edge and high values of ψ_f^B and ψ_p^B ($-30\,^\circ$).

As shown in Fig. 6, the unique solution given by the SORA method is located between the two solutions obtained by the compositions. This method enables disambiguation when modelling the positioning of inserts on tool bodies.

3.5. Description of the cutting edge (E)

The word "edge" should be understood here as the theoretical line defined by the intersection between the rake and clearance faces.

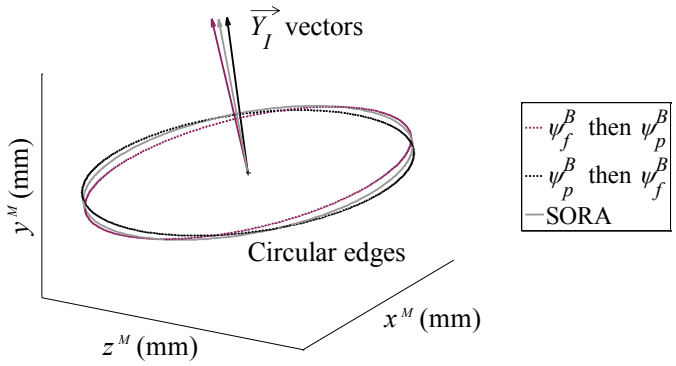

Figure 6: Comparison between SORA method and two matrix compositions: calculated circular cutting edges ($r_\varepsilon = 3$ mm) in $\mathcal{R}_{Machine}$ for $\psi_f^B = \psi_p^B = -30\,^\circ$.

3.5.1. Case of planar cutting edges

In addition to round inserts (ISO R), the ISO designation (ISO 1832) of inserts [49] provides several shapes whose active part is always formed by a nose and two rectilinear edges (major and minor).

Consequently, the edge of ISO inserts can be defined by only two parameters: the nose radius r_ε^E and the tool included angle ε^E (also denoted ε_r when the cutting edge is included in P_r).

A polar description is proposed for all standardised inserts (Fig. 7); the polar angle is denoted θ. If the increment $\Delta\theta$ is constant, the width of the segments varies in the linear portions of the edge; but if $\Delta\theta$ is small enough, this point has no influence.

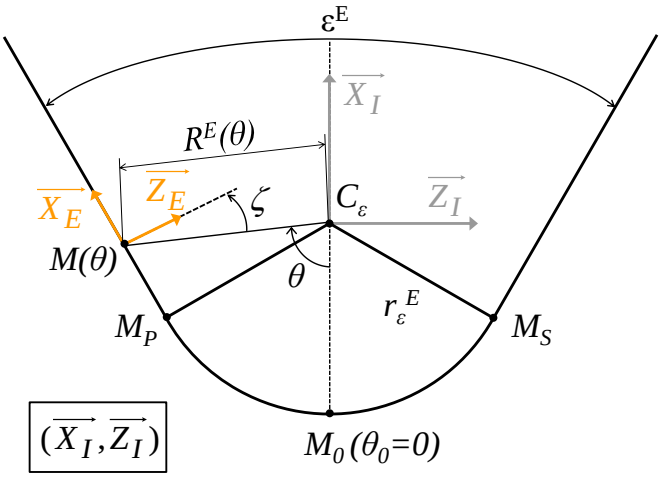

Figure 7: Polar parameterisation of the cutting edge.

The reference angle $\theta_0 = 0°$ is on the bisectrix of the insert; the corresponding point is denoted M_0. Angles θ_P and θ_S (Eq. (7)) define respectively the change between the nose and the major (primary) and minor (secondary) cutting edges; the corresponding points are denoted M_P and M_S.

$$\theta_P = -\theta_S = \frac{\pi}{2} - \frac{\varepsilon^E}{2} \tag{7}$$

The polar radius $R^E(\theta)$ defining the line of the edge can be calculated using Eq. (8).

$$R^E(\theta) = \begin{cases} \dfrac{1}{a\ \cos\theta + b_P\ \sin\theta} & \text{if} \quad \theta > \theta_P \\ r_\varepsilon^E \quad \text{if} \quad \theta_S < \theta < \theta_P \\ \dfrac{1}{a\ \cos\theta + b_S\ \sin\theta} & \text{if} \quad \theta < \theta_S \end{cases} \quad \text{with} \quad \begin{cases} a = \dfrac{\sin(\varepsilon^E/2)}{r_\varepsilon^E} \\ b_P = \dfrac{1}{\sin\theta_P}\left(\dfrac{1}{r_\varepsilon^E} - a\ \cos\theta_P\right) \\ b_S = \dfrac{1}{\sin\theta_S}\left(\dfrac{1}{r_\varepsilon^E} - a\ \cos\theta_S\right) \end{cases} \tag{8}$$

Two homogeneous matrices then define the cutting edge (Eq. (9) and (10)).

$$\mathcal{M}_{E1}(\theta) = \begin{pmatrix} \cos(\frac{\pi}{2}-\theta) & 0 & \sin(\frac{\pi}{2}-\theta) & 0 \\ 0 & 1 & 0 & 0 \\ -\sin(\frac{\pi}{2}-\theta) & 0 & \cos(\frac{\pi}{2}-\theta) & 0 \\ 0 & 0 & 0 & 1 \end{pmatrix} \tag{9}$$

$$\mathcal{M}_{E2}(\theta) = \begin{pmatrix} 1 & 0 & 0 & 0 \\ 0 & 1 & 0 & 0 \\ 0 & 0 & 1 & -R^E(\theta) \\ 0 & 0 & 0 & 1 \end{pmatrix} \tag{10}$$

In order to adjust the system tangent to the edge in the linear portions (Fig. 7), a final rotation is needed (Eq. (11)).

$$\mathcal{M}_{E3}(\theta) = \begin{pmatrix} \cos\zeta & 0 & \sin\zeta & 0 \\ 0 & 1 & 0 & 0 \\ -\sin\zeta & 0 & \cos\zeta & 0 \\ 0 & 0 & 0 & 1 \end{pmatrix} \quad \text{with} \quad \zeta(\theta) = \begin{cases} \dfrac{\varepsilon^E}{2} + \theta - \dfrac{\pi}{2} & \text{if} \quad \theta > \theta_P \\ 0 \quad \text{if} \quad \theta_S < \theta < \theta_P \\ -\dfrac{\varepsilon^E}{2} + \theta - \dfrac{\pi}{2} & \text{if} \quad \theta < \theta_S \end{cases} \tag{11}$$

3.5.2. Case of local inclination

Some inserts have a local inclination of the cutting edge, in order to assist chip breakage or to evacuate the chip (for example, aluminium cutters).

In this case, the 3D-line of the cutting edge must be mathematically defined. For example, the cutting edge equation can be expressed in a Cartesian coordinate system or as a function of the curvilinear abscissa [36]. It is also possible to use an interpolation of the full measured cutting edge, as proposed by Lazoglu [30] from a CMM measurement.

3.5.3. Tool centre height adjustment

The point M_0 (corresponding to $\theta = 0$) is assumed to be set at the spindle axis height on the real tool. From the previous transformations, it is possible to determine the coordinates of M_0 (calculation similar to Eq (22)). Then the matrix $\mathcal{M}_{TCH}$ enables the modelled tool to be repositioned (Eq. (12)), as a tool centre height (TCH) adjustment.

$$\mathcal{M}_{TCH} = \begin{pmatrix} 1 & 0 & 0 & 0 \\ 0 & 1 & 0 & -y_{M_0} \\ 0 & 0 & 1 & 0 \\ 0 & 0 & 0 & 1 \end{pmatrix} \tag{12}$$

The matrix describing the shape of the cutting edge is given by the product of the four previous matrices (Eq. (13)), for each discretised element. The coordinate system $\mathcal{R}_{Insert} = (\overrightarrow{X_I}, \overrightarrow{Y_I}, \overrightarrow{Z_I}, C_\varepsilon)$ linked to the insert is changed into several local coordinate systems $\mathcal{R}_{Edge} = (\overrightarrow{X_E}, \overrightarrow{Y_E}, \overrightarrow{Z_E}, M(\theta))$ linked to the cutting edge.

$$\mathcal{M}_{Edge}(\theta) = \mathcal{M}_{E1}(\theta) \times \mathcal{M}_{E2}(\theta) \times \mathcal{M}_{E3}(\theta) \times \mathcal{M}_{TCH} \tag{13}$$

3.6. Parameterisation of the local cutting geometry of the insert - Edge preparation (P)

As exposed in paragraph 2.3, the local forces are often expressed in a coordinate system linked to the rake face. However, many inserts have a local preparation (given by sintering or grinding) in order to have a more or less positive rake angle and a given clearance angle. Currently, the geometrical models of inserted tools proposed in the literature consider only the positioning on the tool body [7, 11, 36], which is not combined with the local geometry of the insert. Han-Min [46] considered both positioning and grinding angles in order to calculate the working cutting angles, but it was done using an approximated method.

The values of the local rake and inclination angles are not specified by the ISO designation of indexable cutters [49]. However, some manufacturers give information on their cutting geometries and edge preparations [47]. The local normal rake angle can be either positive or negative (for example, if the edge preparation is a chamfer).

Three local angles can be used to define the geometry (Fig. 8): an inclination angle λ^E, together with a rake angle γ_n^P or a clearance angle α_n^P, depending on whether the rake or clearance face is considered. The values of these angles may vary along the cutting edge.

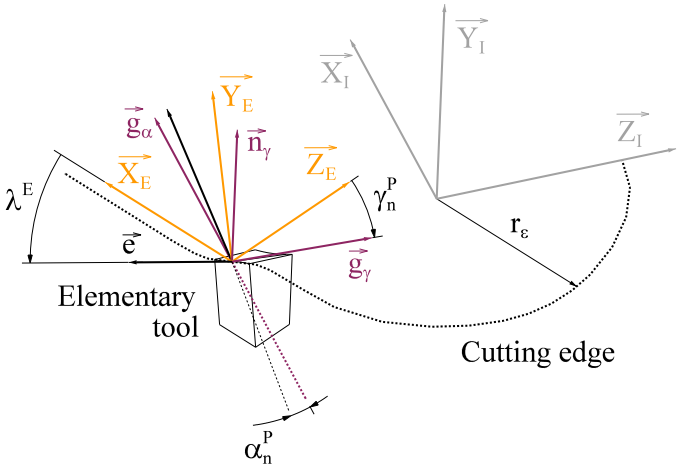

Figure 8: Local geometry of the insert.

In the case of local inclination, the basis must be tilted according to Eq. (14) in order to be tangent to the inclined edge. For the current point M_j, the local inclination angle λ^E is equal to the angle between vector $\overrightarrow{M_{j-1}M_{j+1}}$ and the plane $(\overrightarrow{X_I}, \overrightarrow{Z_I})$; λ^E is positive if $\overrightarrow{M_{j-1}M_{j+1}} \cdot \overrightarrow{Y_I} < 0$.

$$\mathcal{M}_\lambda(\theta) = \begin{pmatrix} \cos(-\lambda^E) & -\sin(-\lambda^E) & 0 & 0 \\ \sin(-\lambda^E) & \cos(-\lambda^E) & 0 & 0 \\ 0 & 0 & 1 & 0 \\ 0 & 0 & 0 & 1 \end{pmatrix} \tag{14}$$

The local normal rake γ_n^P and clearance α_n^P angles can then be taken into account (Eq. (15) and (16)).

$$\mathcal{M}_\gamma^P = \begin{pmatrix} 1 & 0 & 0 & 0 \\ 0 & \cos\gamma_n^P & -\sin\gamma_n^P & 0 \\ 0 & \sin\gamma_n^P & \cos\gamma_n^P & 0 \\ 0 & 0 & 0 & 1 \end{pmatrix} \tag{15}$$

$$\mathcal{M}_\alpha^P = \begin{pmatrix} 1 & 0 & 0 & 0 \\ 0 & \cos\alpha' & -\sin\alpha' & 0 \\ 0 & \sin\alpha' & \cos\alpha' & 0 \\ 0 & 0 & 0 & 1 \end{pmatrix} \quad \text{with} \quad \alpha' = -\frac{\pi}{2} - \alpha_n^P \tag{16}$$

It is also possible to use a corrected rake angle for low uncut chip thicknesses [50, 51], in order to model the effect of rounded cutting edges. In this case, the calculation of the uncut chip thickness (detailed in Section 5.2) must be performed between the calculation of the cutting edge (Eq. (13)) and the transformation $\mathcal{M}_\gamma^P$.

Matrices $\mathcal{M}_\gamma$ and $\mathcal{M}_\alpha$ can be then calculated by composition (Eq. (17) and (18)) in order to obtain coordinate systems $\mathcal{R}_\gamma = (\overrightarrow{e}, \overrightarrow{n_\gamma}, \overrightarrow{g_\gamma}, M)$ and $\mathcal{R}_\alpha = (\overrightarrow{e}, \overrightarrow{n_\alpha}, \overrightarrow{g_\alpha}, M)$, respectively linked to the rake and clearance faces.

$$\mathcal{M}_\gamma(\theta) = \mathcal{M}_\lambda(\theta) \times \mathcal{M}_\gamma^P(\theta) \tag{17}$$

$$\mathcal{M}_\alpha(\theta) = \mathcal{M}_\lambda(\theta) \times \mathcal{M}_\alpha^P(\theta) \tag{18}$$

3.7. Chip flow angle

A local chip flow angle η can be consider in the transformations to introduce a realistic friction force $\overrightarrow{f_{f\,\gamma}}$ on the rake face [35]. The relative transformation is given by Eq. (19).

$$\mathcal{M}_\eta = \begin{pmatrix} \cos\eta & 0 & \sin\eta & 0 \\ 0 & 1 & 0 & 0 \\ -\sin\eta & 0 & \cos\eta & 0 \\ 0 & 0 & 0 & 1 \end{pmatrix} \tag{19}$$

This local change can be due to the local working cutting edge inclination angle λ_{se} [35, 52] and also to the working cutting edge angle κ_{re} [6].

4. Representation of the cutting geometry

Depending on the chosen local cutting model, several local coordinate systems may be needed:

- $\mathcal{R}_{ovh} = (\overrightarrow{o}, \overrightarrow{v}, \overrightarrow{h}, M)$ if the model considers the forces $\overrightarrow{f_v}$ and $\overrightarrow{f_h}$ (Fig. 1(a));
- $\mathcal{R}_\gamma = (\overrightarrow{e}, \overrightarrow{n_\gamma}, \overrightarrow{g_\gamma}, M)$ if the forces $\overrightarrow{f_{n\gamma}}$ and $\overrightarrow{f_{g\gamma}}$ are applied on the rake face with no chip flow angle (Fig. 1(b));
- $\mathcal{R}_\eta = (\overrightarrow{o_\gamma}, \overrightarrow{n_\gamma}, \overrightarrow{f_\gamma}, M)$ if the friction force is applied in the local chip flow direction;
- $\mathcal{R}_\alpha = (\overrightarrow{e}, \overrightarrow{n_\alpha}, \overrightarrow{g_\alpha}, M)$ if the contact on the clearance face is taken into account (Fig. 1(c)); however, the friction direction corresponds to the projection of $\overrightarrow{v_e}$ on $\mathcal{A}_\alpha$.

The calculation of the coordinate system $\mathcal{R}_\gamma$ is explained hereafter (Eq. (20) to (23)).

The geometry of the tool is set for a given operation; for each tool discretisation element, the matrix $\mathcal{M}_{Tool}$ (Eq. (20)) can be calculated only once, while the matrix of the machine movements $\mathcal{M}_{Machine}$ must be changed at each spindle revolution k (or each time step).

$$\mathcal{M}_{Tool\,\gamma}(\theta) = \mathcal{M}_{Body} \times \mathcal{M}_{Edge}(\theta) \times \mathcal{M}_\gamma(\theta) \tag{20}$$

The matrix relative to the whole cutting operation $\mathcal{M}_{Op}$ is given by Eq. (21).

$$\mathcal{M}_{Op}(k,\theta) = \mathcal{M}_{Machine}(k) \times \mathcal{M}_{Tool\,\gamma}(\theta) \tag{21}$$

Then the coordinates of the current points M (Eq. (22)) and of the local vectors (Eq. (23)) expressed in $\mathcal{R}_{Machine}$ can be calculated.

$$M(k,\theta) = \begin{bmatrix} x(k,\theta) \\ y(k,\theta) \\ z(k,\theta) \\ 1 \end{bmatrix}_{\mathcal{R}_{Machine}} = \mathcal{M}_{Op}(k,\theta) \times \begin{bmatrix} 0 \\ 0 \\ 0 \\ 1 \end{bmatrix}_{\mathcal{R}_\gamma} \tag{22}$$

$$\begin{cases} \overrightarrow{e}(\theta) = \begin{bmatrix} x_e(\theta) \\ y_e(\theta) \\ z_e(\theta) \\ 1 \end{bmatrix}_{\mathcal{R}_{Machine}} = \mathcal{M}_{Op}(k,\theta) \times \begin{bmatrix} 1 \\ 0 \\ 0 \\ 0 \end{bmatrix}_{\mathcal{R}_\gamma} \\ \overrightarrow{n_\gamma}(\theta) = \begin{bmatrix} x_{n_\gamma}(\theta) \\ y_{n_\gamma}(\theta) \\ z_{n_\gamma}(\theta) \\ 1 \end{bmatrix}_{\mathcal{R}_{Machine}} = \mathcal{M}_{Op}(k,\theta) \times \begin{bmatrix} 0 \\ 1 \\ 0 \\ 0 \end{bmatrix}_{\mathcal{R}_\gamma} \\ \overrightarrow{g_\gamma}(\theta) = \begin{bmatrix} x_{g_\gamma}(\theta) \\ y_{g_\gamma}(\theta) \\ z_{g_\gamma}(\theta) \\ 1 \end{bmatrix}_{\mathcal{R}_{Machine}} = \mathcal{M}_{Op}(k,\theta) \times \begin{bmatrix} 0 \\ 0 \\ 1 \\ 0 \end{bmatrix}_{\mathcal{R}_\gamma} \end{cases} \tag{23}$$

Three-dimensional representations[1] are shown in Fig. 9 for different types of inserts and bodies. The numerical values of the parameters correspond either to the ISO designation [49] or to the data given by the tool manufacturer Sandvik [47].

The examples in Fig. 9 are the following:

[1] Only the vectors $\overrightarrow{g_\gamma}$ and $-\overrightarrow{g_\alpha}$ are represented (cf. Fig. 8).

- Case (a): a positive basic shape insert DCMT 11T308-UF ($\varepsilon^E = 55°, r_\varepsilon^E = 0.8$ mm$, \alpha_n^P = 7°, \gamma_n^P = 6°$) non-inclined by the body SDHCL 2020 K11 ($\kappa_r^B = 107.5°, \psi_f^B = 0°, \psi_p^B = 0°$);
- Case (b): a negative basic shape insert CNMG 120408-23 with a positive cutting geometry due to the edge preparation ($\varepsilon^E = 80°, r_\varepsilon^E = 0.8$ mm$, \alpha_n^P = 0°, \gamma_n^P = 13°$) twice tilted by the body PCLNL 2020 K12 ($\kappa_r^B = 95°, \psi_f^B = -6°, \psi_p^B = -6°$);
- Case (c): a negative basic shape insert SNGN 120408-T02520 with a chamfered edge preparation ($\varepsilon^E = 90°, r_\varepsilon^E = 0.8$ mm$, \alpha_n^P = 0°, \gamma_n^P = -20°$) once tilted by the body CSSNL 2525M12-4 ($\kappa_r^B = 45°, \psi_f^B = -8°, \psi_p^B = 0°$).

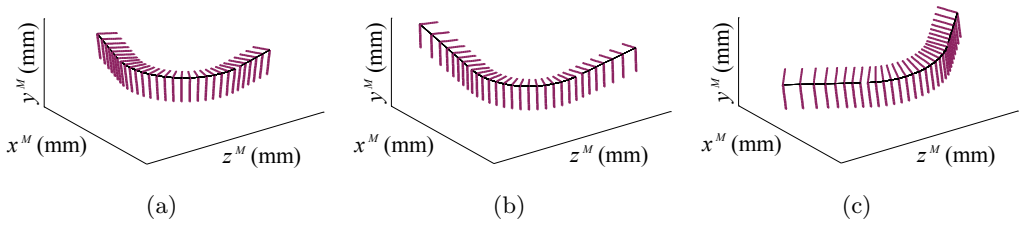

Figure 9: 3D representations of the cutting geometry in $\mathcal{R}_{Machine}$ for different insert-body pairs: (a) DCMT-UF + SDHCL; (b) CNMG-23 + PCLNL; (c) SNGN-T (chamfered) + CSSNL.

5. Calculation of the local cutting parameters

The geometry of the tool can be used to orient the local forces. In addition, local cutting parameters can be used as inputs in the expression of the local cutting relations.

The cutting parameters can be sorted as follows:

- the local cutting conditions: V_c, h;
- the local working cutting angles: γ_{ne}, λ_{se}, α_{oe};
- the local cutting edge characteristics given by the global geometry of the insert, κ_{re} and the edge curvature (primarily r_ε^E for turning tools); this point means that the segments are not considered as independent;
- the edge properties: r_β in the case of a honed edge or chamfer dimensions, roughness and tool material or coating;
- the local workpiece curvatures.

5.1. Local effective cutting speed $\vec{v_e}$

In turning, the cutting movement is given by the workpiece rotation. In the case of non-planar cutting edges or inclined inserts, since the current cutting point M is not in the plane $(O_{Pr}, \overrightarrow{X_M}, \overrightarrow{Z_M})$, the local cutting speed $\overrightarrow{v_c}$ is not parallel to $\overrightarrow{Y_M}$.

The direction and norm of $\overrightarrow{v_c}$ can be calculated according to Eq. (24) from the spindle speed N and the coordinates of the current point.

$$\overrightarrow{v_c} = ||\overrightarrow{v_c}|| \cdot \overrightarrow{v_u} \quad \text{with} \quad \begin{cases} ||\overrightarrow{v_c}|| = \dfrac{\pi}{500}\sqrt{x^2(\theta)+y^2(\theta)}\,N \\ \overrightarrow{v_u} = \dfrac{1}{\sqrt{x^2(\theta)+y^2(\theta)}} \begin{bmatrix} -y(\theta) \\ x(\theta) \\ 0 \\ 0 \end{bmatrix}_{\mathcal{R}_{Machine}} \end{cases} \tag{24}$$

Then the local effective cutting speed $\overrightarrow{v_e}$ can be calculated (Eq. (25)).

$$\overrightarrow{v_e} = \overrightarrow{v_c} + \frac{\overrightarrow{V_f}}{1000} \tag{25}$$

5.2. Uncut chip thickness

The local thickness of cut h_j is defined for each point M_j of the active cutting edge. The measurement direction of h is the intersection of planes P_{ne} and P_{re} [2]. Thus it results from a three-dimensional calculation.

5.2.1. Cylindrical turning with a cutting edge included in P_r

Analytical calculation is of interest when identification algorithms are used, to reduce the calculation time. It is possible in the case of a planar and non-inclined cutting edge ($\psi_p^B = \psi_f^B = 0°$), and if the considered operation is simple (cylindrical turning or facing, for example).

Armarego and Samaranayake [53] have counted nine types of cut shapes in cylindrical turning, while Atabey et al. [54] have studied the case of boring. Each configuration should be considered in detail.

As the edge is included in P_r, the classical notations κ_r, ε_r and r_ε are used in this section instead of κ_r^B, ε^E and r_ε^E.

The change of variable $\Theta = \theta + \kappa_r + \varepsilon_r/2 - \pi/2$ is helpful to compare uncut chip thicknesses between different tools.

The analytical calculation of h is developed for cylindrical turning in the following paragraphs. In this particular case, Θ is equal to κ_{re}.

Circular cutting edge

In 1989, the case where only the nose is cutting was studied in detail by Moriwaki and Okuda [55]; this configuration is of prime importance since it corresponds to finishing operations. In this particular case, the maximum uncut chip thickness on the active cutting edge during cylindrical turning can be calculated by Eq. (26) [23].

$$h_{max} = r_\varepsilon - \sqrt{(\sqrt{r_\varepsilon^2 - (r_\varepsilon - a_p)^2} - f)^2 + (r_\varepsilon - a_p)^2} \tag{26}$$

Here the active cutting edge is delimited by angles Θ_{Min} and Θ_{Max}, given by Eq. (27) and (28).

$$\Theta_{Min} = \arcsin\left(\frac{-f}{2\ r_\varepsilon}\right) \tag{27}$$

$$\Theta_{Max} = \arccos\left(\frac{r_\varepsilon - a_p}{r_\varepsilon}\right) \tag{28}$$

The local uncut chip thickness along the active cutting edge can then be calculated using Eq. (29) (see also [53] or [51] for a front turret lathe).

$$\begin{cases} \text{If } \Theta < \Theta_{h_{max}} : \quad h(\Theta) = r_\varepsilon + f\ \sin\Theta - \sqrt{r_\varepsilon^2 - f^2\ \cos^2(\Theta)} \\ \text{If } \ \Theta > \Theta_{h_{max}} : \quad h(\Theta) = r_\varepsilon - \dfrac{r_\varepsilon - a_p}{\cos\Theta} \\ \text{with} \quad \Theta_{h_{max}} = \arccos\left(\dfrac{r_\varepsilon - a_p}{r_\varepsilon - h_{max}}\right) \end{cases} \tag{29}$$

Other planar edge shapes

Depending on the values of the cutting parameters (f and a_p) and the characteristics of the tool (r_ε, ε_r and κ_r), five zones can be identified in the area of cut, as shown in Fig. 10. These correspond to the more complex cases, when a_p and f are larger than the limit values given by Eq. (30) and (31) [53].

$$a_{plim} = r_\varepsilon\ (1 - \cos\kappa_r) \tag{30}$$

$$f_{lim} = 2\ r_\varepsilon\ \sin(\kappa_r + \varepsilon_r) \tag{31}$$

The formulae for the calculation of the characteristic angles Θ, shown in Fig. 10, are given in Appendix A, while the calculation of the uncut chip thickness is detailed in Appendix B.

It should be noted that the equation $h = f\ \sin\kappa_r$ is too often misused [11], since it is only available in zone II. Also, for $\kappa_r > 90°$, zone I is removed with the chip, without being cut.

Two numerical applications are proposed in Fig. 11 (with the same cutting parameters: $f = 0.3$ mm/rev and $a_p = 1$ mm):

- (a) a DCMT11T304 insert ($r_\varepsilon = 0.4$ mm; $\varepsilon_r = 55°$) on a SDHCL body ($\kappa_r = 107.5°$);
- (b) a SCMT120404 insert ($r_\varepsilon = 0.4$ mm; $\varepsilon_r = 90°$) on a SSDCL body ($\kappa_r = 45°$).

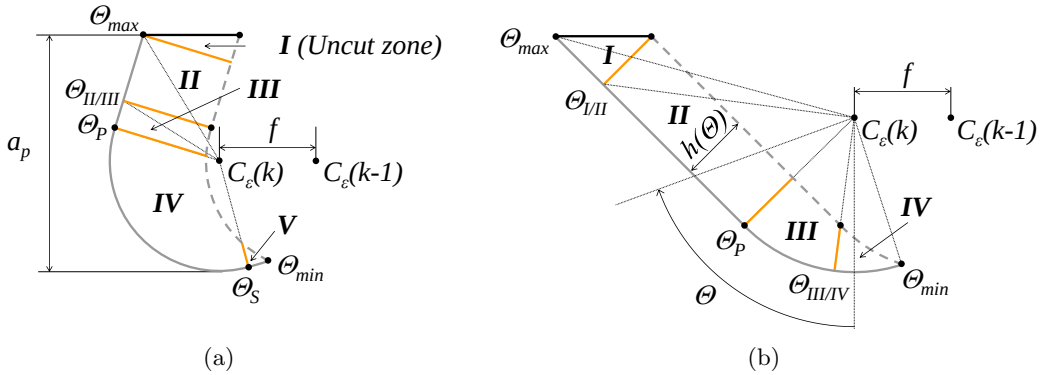

(a) (b)

Figure 10: Cutting zones for cylindrical turning with a rhombic insert, for two cases: (a) $\kappa_r > 90°$ ($a_p > a_{p\,lim}$ and $f > f_{lim}$); (b) $\kappa_r < 90°$ ($a_p > a_{p\,lim}$ but $f < f_{lim}$).

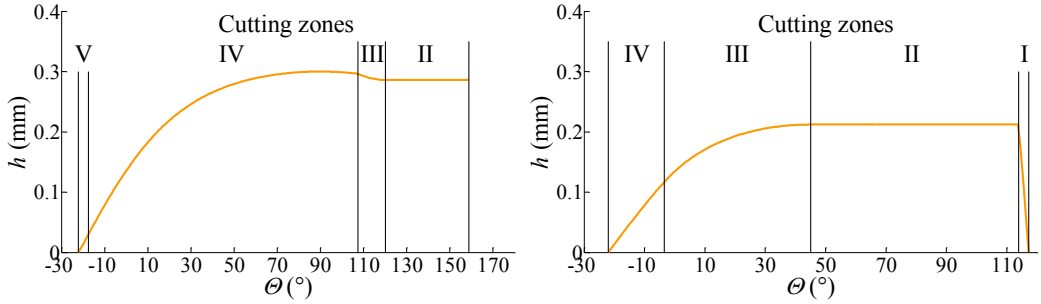

(a) (b)

Figure 11: Uncut chip thickness along the active cutting edge: (a) DCMT11T304 + SDHCL; (b) SCMT120404 + SSDCL.

Knowledge of the uncut chip thickness is obviously required for the calculation of the cutting forces, but it also provides information on the mechanical load of the tool. Thus it is possible to forecast the zones of the cutting tool where the wear will be the greatest.

5.2.2. General case

Strictly, when the cutting edge is inclined, the uncut chip thickness should be calculated between the cutting edge and the surface generated at the previous revolution [56]. However, the calculation can be approximated in the plane $(O_{Pr}, \overrightarrow{X_M}, \overrightarrow{Z_M})$ in some cases. Indeed, the difference is negligible insomuch as the workpiece diameter is large, and the feed and the inclination are small.

The simulation of contour turning operations, or with non-ISO inserts like wiper inserts, nevertheless requires the calculation of the uncut chip thickness with various shapes of tool-workpiece intersections. As all cases of tool-workpiece intersection cannot be predicted, it is simpler to evaluate h by numerical methods. The methods currently used are:

- point-to-point distances [8, 9];
- N-buffers [14];
- dexel or voxel removal [6, 30];
- volumic boolean operations [10].

It is thus possible to simulate the forces along a tool path by numerical calculation of the uncut chip thickness, even if the identification of the model has been performed from cylindrical turning tests (with an analytical calculation of h).

5.3. Working cutting angles

From the previous calculations of the local coordinate systems and $\overrightarrow{v_e}$, it is possible to define the planes of the tool-in-use system (Eq. (32)) [1].

$$\begin{cases} P_{re} \perp \overrightarrow{v_e} \\ P_{fe} = (\overrightarrow{v_c}, \overrightarrow{V_f}) \\ P_{se} = (\overrightarrow{v_e}, \overrightarrow{e}) \\ P_{oe} = (\overrightarrow{v_e}, \overrightarrow{h}) \\ P_{ne} = (\overrightarrow{n_\gamma}, \overrightarrow{g_\gamma}) = P_n \end{cases} \tag{32}$$

According to Armarego [52], the normal rake angle γ_n is the most relevant rake angle; this conclusion has been confirmed more recently by Komandury et al. [57].

As elastic recovery occurs normally to the machined surface, and because the friction on the clearance face is due to the primary motion, the working orthogonal clearance angle α_{oe} seems to have the most physical meaning.

The inclination angle λ_{se} and the cutting edge angle κ_{re} may influence both the chip flow direction and the value of the forces.

The angles of the tool-in-use system can be calculated by Eq. (33). The notation $\overrightarrow{v_e}^{\perp P_n}$ indicates the orthogonal projection of vector $\overrightarrow{v_e}$ on plane P_n.

$$\begin{cases} \gamma_{ne} = (\widehat{A_\gamma, P_{re}})_{P_{ne}} = (\widehat{\overrightarrow{v_e}^{\perp P_n}, \overrightarrow{n_\gamma}}) \\ \alpha_{ne} = (\widehat{A_\alpha, P_{se}})_{P_{ne}} = (\widehat{\overrightarrow{v_e}^{\perp P_n}, \overrightarrow{g_\alpha}}) \\ \lambda_{se} = (\widehat{P_{re}, \overrightarrow{e}})_{P_{se}} = (\widehat{\overrightarrow{v_e}, \overrightarrow{e}}) - \dfrac{\pi}{2} \\ \kappa_{re} = (\widehat{P_{se}, P_{fe}})_{P_{re}} = \mathrm{sgn}(\overrightarrow{e} \cdot \overrightarrow{X_M})\ (\widehat{\overrightarrow{v_f}^{\perp P_{re}}, \overrightarrow{e}^{\perp P_{re}}}) \\ \alpha_{oe} = \arctan(\tan\alpha_{ne}\ \cos\lambda_{se}) \end{cases} \tag{33}$$

Fig. 12 shows the evolution of the working angles along the cutting edge in cylindrical turning with the following parameters:

- a CNMG 120408-23 / PCLNL 2020 K12 pair for the tool (idem Fig. 9 (b));
- $V_c = 100$ m/min and $D = 100$ mm ($N = 318$ rev/min);
- $f = 0.3$ mm/rev ($V_f = 95$ mm/min) and $a_p = 2$ mm.

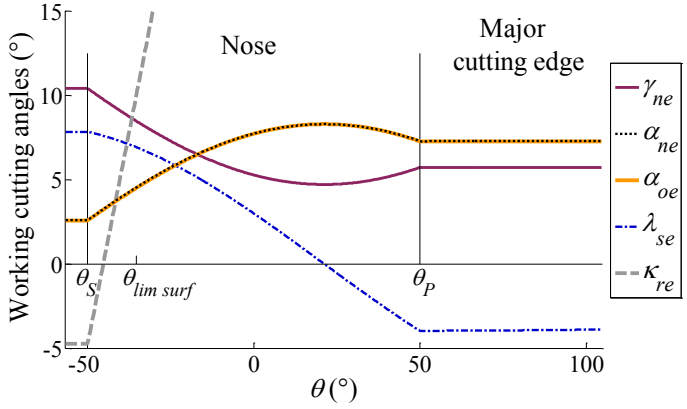

Figure 12: Calculated working cutting angles along the active cutting edge.

This type of result allows the local working cutting geometry to be analysed. For example, in Fig. 12, it can be seen that the working normal rake angle γ_{ne} is greater for small values of θ. Yet this portion of the edge is where the smaller uncut chip thicknesses are and where the machined surface is generated ($\theta < \theta_{lim\,surf}$). Thus, the working cutting geometry tends to improve the cut in this zone and therefore a better surface finish can be expected.

In the same vein, the geometrical model can be used when designing tools in order to produce a given working geometry, as proposed by Hsieh for single-point cutting tools [58]. Thus a variable local clearance angle α_n^P would allow the normal wedge angle β_n to be maximised where the chip thickness is the largest while having a constant working clearance angle α_{ne}.

6. Calculation of global forces and moments by numerical integration

When the local cutting forces are expressed in the RTA basis (Fig. 1 (a)), the summation is obvious [29]. But, when they are applied on the rake and clearance faces (Fig. 1 (c)), they have to be projected before

numerical summation.

As the vectors $\overrightarrow{n_\gamma}$, $\overrightarrow{g_\gamma}$, $\overrightarrow{n_\alpha}$ and $\overrightarrow{g_\alpha}$ are expressed in $\mathcal{R}_{Machine}$ (Eq. (23)), the projections on $\overrightarrow{X_M}$, $\overrightarrow{Y_M}$ and $\overrightarrow{Z_M}$ are direct.

The calculation for the component F_x of the force and the moment around $\overrightarrow{X_M}$ at point C_ε are respectively given by Eq. (34) and (35) for the case corresponding to Fig. 1 (c). L_s is the length of the segment, which is variable on the rectilinear edges.

$$F_x(k) = \sum_{i=\alpha,\gamma} \sum_{j=1}^{N_{seg}} f_{n\,i}(\theta_j)\ L_s(\theta_j)\ \overrightarrow{n_i}(\theta_j)\ \cdot\ \overrightarrow{X_M} + f_{g\,i}(\theta_j)\ L_s(\theta_j)\ \overrightarrow{g_i}(\theta_j)\ \cdot\ \overrightarrow{X_M} \tag{34}$$

$$\mathcal{M}_{x,C_\varepsilon}(k) = \sum_{i=\alpha,\gamma} \sum_{j=1}^{N_{seg}} f_{n\,i}(\theta_j)\ L_s(\theta_j)\ (\overrightarrow{n_i}(\theta_j)\ \wedge\ \overrightarrow{M_jC_\varepsilon})\ \cdot\ \overrightarrow{X_M} + f_{g\,i}(\theta_j)\ L_s(\theta_j)\ (\overrightarrow{g_i}(\theta_j)\ \wedge\ \overrightarrow{M_jC_\varepsilon})\ \cdot\ \overrightarrow{X_M} \tag{35}$$

This calculation must be made at each translation of the tool, corresponding to one revolution of the spindle.

7. Conclusion

In this paper, a generalised geometrical model of turning operations is proposed. The geometrical transformations linked to the machine-tool, the tool body and the insert are modelled by homogeneous matrices.

This contribution should be considered as a methodology, which facilitates the application of cutting force models to the various cutting operations. In order to develop an algorithm for cutting force calculation, whole or parts of transformations must be written step-by-step.

The variables required in the cutting relations can then be easily evaluated and the global forces applied on the tool can be calculated by integration.

The geometrical results can also be helpful for designing cutting tools in order to increase their life expectancy.

An important feature of this work is the consideration of both the local geometry of the insert and its positioning, modelled by the SORA method, which allows a unique solution to be calculated from the information provided by the tool manufacturers.

However, as noted by Armarego [40] more than 10 years ago, the geometry and the specification of the tools have to be clearly defined by the standards and the tool manufacturers. Currently, the definition of the positioning of indexable inserts and of local rake geometry remains fuzzy.

Appendix A. Angles Θ defining the cut for cylindrical turning with non-rounded ISO inserts

Intrinsic angles of the tool:

$$\Theta_P = \kappa_r \tag{A.1}$$

$$\Theta_S = -\kappa'_r = \kappa_r + \varepsilon_r - \pi \tag{A.2}$$

Limit angles if the minor and major edges are active (if the limits are in the nose, the expressions of Θ_{Max} and Θ_{Min} are equal to those given by Eq. (27) and (28) for round inserts):

$$\Theta_{Max} = \arctan\left[\frac{a_p + r_\varepsilon\ (\cos\kappa_r - 1)}{r_\varepsilon\ \sin\kappa_r}\right] + \kappa_r \tag{A.3}$$

$$\Theta_{Min} = -\arctan\left[\frac{f}{r_\varepsilon}\ \cos\kappa'_r - \frac{\sqrt{r_\varepsilon^2 - (r_\varepsilon - f\ \sin\kappa'_r)^2}}{r_\varepsilon}\right] - \kappa'_r \tag{A.4}$$

Characteristic angles if $\kappa_r < 90°$:

$$\Theta_{I/II} = \arctan\left[\frac{a_p + r_\varepsilon\ (\cos\kappa_r - 1) - f\ \cos\kappa_r\ \sin\kappa_r}{r_\varepsilon\ \sin\kappa_r}\right] + \kappa_r \tag{A.5}$$

$$\Theta_{III/IV} = \arctan\left[\frac{r_\varepsilon\ \sin\kappa_r - f}{r_\varepsilon\ \cos\kappa_r}\right] \tag{A.6}$$

Characteristic angles if $\kappa_r > 90°$:

$$\Theta_{II/III} = \arctan\left[\frac{r_\varepsilon + f\ \sin\kappa_r}{f\ \cos\kappa_r - r_\varepsilon\ \tan\kappa_r}\right] + \frac{\pi}{2} \tag{A.7}$$

Appendix B. Uncut chip thickness *h* along the active cutting edge

- In zone V:

$$h_V = R^E(\theta)\ \cos(\kappa'_r + \Theta) - f\ \sin\kappa'_r - \sqrt{r_\varepsilon^2 - [f\ \cos\kappa'_r + R^E(\theta)\ \sin(\kappa'_r + \Theta)]^2} \tag{B.1}$$

- In zone IV:

$$h_{IV} = r_\varepsilon + f\ \sin\Theta - \sqrt{r_\varepsilon^2 - f^2\ \cos^2\Theta} \tag{B.2}$$

- In zone III:

$$h_{III} = \begin{cases} r_\varepsilon - \dfrac{r_\varepsilon - f\ \sin\kappa_r}{\cos(\kappa_r - \Theta)} & \text{if } \kappa_r < 90° \\ R^E(\theta)\ \cos(\kappa_r - \Theta) + f\ \sin\kappa_r & \\ -\sqrt{r_\varepsilon^2 - [f\ \cos\kappa_r - R^E(\theta)\ \sin(\kappa_r - \Theta)]^2} & \text{if } \kappa_r > 90° \end{cases} \tag{B.3}$$

- In zone II:

$$h_{II} = f\ \sin\kappa_r \tag{B.4}$$

- In zone I:

$$h_I = \begin{cases} f\ \sin\kappa_r \left[1 - \dfrac{R^E(\theta_{I/II})\ \cos\Theta_{I/II} - R^E(\theta)\ \cos\Theta}{\cos\kappa_r\ \sqrt{f^2\ (1 - \sin^2\kappa_r)}}\right] & \text{if } \kappa_r < 90° \\ \text{Uncut zone if } \kappa_r > 90° \end{cases} \tag{B.5}$$

References

[1] ISO, Basic quantities in cutting and grinding - part 1, ISO 3002-1, 1982.
[2] ISO, Basic quantities in cutting and grinding - part 3, ISO 3002-3, 1984.
[3] ISO, Industrial automation systems and integration - numerical control of machines - coordinate system and motion nomenclature, ISO 841, 2001.
[4] M. H. Raffles, K. Kolluru, D. Axinte, H. Llewellyn-Powell, Assessment of adhesive fixture system under static and dynamic loading conditions, Proc. of the IMechE, Part B: J. Eng. Manuf. 227/2 (2013) 267–280.
[5] E. Budak, Y. Altintas, Modeling and avoidance of static form errors in peripheral milling of plates, Int. J. Mach. Tools Manuf. 35/3 (1995) 459–476.
[6] S. G. Kapoor, R. E. DeVor, R. Zhu, R. Gajjela, G. Parakkal, D. Smithey, Development of mechanistic models for the prediction of machining performance: Model building methodology, Mach. Sci. Technol. 2/2 (1998) 213–238.
[7] S. Engin, Y. Altintas, Mechanics and dynamics of general milling cutters. part ii: Inserted cutters, Int. J. Mach. Tools Manuf. 41/15 (2001) 2213–2231.
[8] H. Paris, G. Peigne, R. Mayer, Surface shape prediction in high speed milling, Int. J. Mach. Tools Manuf. 44/15 (2004) 1567–1576.
[9] E. Rivière-Lorphèvre, Etude et simulation de procédés de fraisage grande vitesse : efforts de coupe, stabilité, états de surface (in French), Ph.D. thesis, Faculté Polytechnique de Mons, 2007.
[10] D. Biermann, P. Kersting, T. Surmann, A general approach to simulating workpiece vibrations during five-axis milling of turbine blades, CIRP Ann. - Manuf. Technol. 59/1 (2010) 125–128.
[11] Y. Altintas, Z. M. Kilic, Generalized dynamic model of metal cutting operations, CIRP Ann. - Manuf. Technol. 62/1 (2013) 47–50.
[12] F. Valiorgue, J. Rech, H. Hamdi, P. Gilles, J. M. Bergheau, A new approach for the modelling of residual stresses induced by turning of 316l, J. Mater. Process. Technol. 191/1–3 (2007) 270–273.
[13] J. Gravier, V. Vignal, S. Bissey-Breton, Influence of residual stress, surface roughness and crystallographic texture induced by machining on the corrosion behaviour of copper in salt-fog atmosphere, Corros. Sci. 61 (2012) 162–170.
[14] B. K. Fussell, R. B. Jerard, J. G. Hemmett, Robust feedrate selection for 3-axis nc machining using discrete models, J. Manuf. Sci. Eng. 123/2 (2001) 214–224.
[15] B. U. Guzel, I. Lazoglu, Increasing productivity in sculpture surface machining via off-line piecewise variable feedrate scheduling based on the force system model, Int. J. Mach. Tools Manuf. 44/1 (2004) 21–28.
[16] S. Saikumar, M. Shunmugam, Development of a feed rate adaption control system for high-speed rough and finish end-milling of hardened en24 steel, Int. J. Adv. Manuf. Technol. 59/9 (2012) 869–884.
[17] C. A. van Luttervelt, T. H. C. Childs, I. S. Jawahir, F. Klocke, P. K. Venuvinod, Y. Altintas, et al., Present situation and future trends in modelling of machining operations - progress report of the cirp working group "modelling of machining operations", CIRP Ann. - Manuf. Technol. 47/2 (1998) 587–626.

[18] K. F. Ehmann, S. G. Kapoor, R. E. DeVor, I. Lazoglu, Machining process modeling: A review, J. Manuf. Sci. Eng. 119/4B (1997) 655–663.
[19] R. G. Reddy, S. G. Kapoor, R. E. DeVor, A mechanistic force model for contour turning, J. Manuf. Sci. Eng. 122/3 (2000) 398–405.
[20] M. Wang, B. Xu, S. Dong, J. Zhang, S. Wei, Experimental investigations of cutting parameters influence on cutting forces in turning of fe-based amorphous overlay for remanufacture, Int. J. Adv. Manuf. Technol. 65/5–8 (2013).
[21] T. Carlsson, T. Stjernstoft, B. Lindström, A model for calculation of the geometrical shape of the cutting tool - workpiece interface, CIRP Ann. - Manuf. Technol. 50/1 (2001) 41–44.
[22] B. Denkena, J. Köhler, Consideration of the form of the undeformed section of cut in the calculation of machining forces, Mach. Sci. Technol. 14/4 (2010) 455–470.
[23] Y. Huang, S. Y. Liang, Force modelling in shallow cuts with large negative rake angle and large nose radius tools - application to hard turning, Int. J. Adv. Manuf. Technol. 22/9 (2003) 626–632.
[24] A. J. P. Sabberwal, Chip section and cutting force during the milling operation, Ann. of the CIRP 10/3 (1961) 197–203.
[25] E. J. A. Armarego, C. Y. Cheng, Drilling with flat rake face and conventional twist drills - i. theoretical investigation, Int. J. Mach. Tool Des. Res. 12/1 (1972) 17–35.
[26] J. Tlusty, P. MacNeil, Dynamics of cutting forces in end milling, Ann. of the CIRP 24/1 (1975) 21–25.
[27] L. V. Colwell, Predicting the angle of chip flow for single point cutting tools, Trans. of the ASME 76/2 (1954) 199–204.
[28] M. C. Shaw, N. H. Cook, P. A. Smith, The mechanics of three-dimensional cutting operations, Trans. of the ASME 74 (1952) 1055–1064.
[29] Y. Altintas, Manufacturing Automation: Metal Cutting Mechanics, Machine Tool Vibrations, and CNC Design, Cambridge University Press, 2000.
[30] I. Lazoglu, Sculpture surface machining: a generalized model of ball-end milling force system, Int. J. Mach. Tools Manuf. 43/5 (2003) 453–462.
[31] S. Bissey, G. Poulachon, F. Lapujoulade, J. Giessler, M. Demesy, Optimization of milling cutter geometries for hsc-machining, Proc. of the 4th Int. Conf. on Met. Cut. and High Speed Mach., Darmstadt, Germany (2003).
[32] E. Thomsen, J. Lapsley, R. Grassi, Deformation work absorbed by the workpiece during metal cutting, Trans. of the ASME 75 (1953) 591–603.
[33] E. J. A. Armarego, C. J. Epp, An investigation of zero helix peripheral up-milling, Int. J. Mach. Tool Des. Res. 10/2 (1970) 273–291.
[34] E. J. A. Armarego, R. C. Whitfield, Computer based modelling of popular machining operations for force and power prediction, CIRP Ann. - Manuf. Technol. 34/1 (1985) 65–69.
[35] S. Bissey-Breton, G. Poulachon, F. Lapujoulade, Integration of tool geometry in prediction of cutting forces during milling of hard materials, Proc. of the IMechE, Part B: J. Eng. Manuf. 220/4 (2006) 579–587.
[36] M. Kaymakci, Z. M. Kilic, Y. Altintas, Unified cutting force model for turning, boring, drilling and milling operations, Int. J. Mach. Tools Manuf. 54-55 (2012) 34–45.
[37] G. Yücesan, Y. Altintas, Prediction of ball end milling forces, J. Eng. Ind. 118/1 (1996) 95–103.
[38] S. Campocasso, J. P. Costes, G. Poulachon, A. Perez-Duarte, Cutting forces modeling in finish turning of inconel 718 alloy with round inserts, Proc. of the 13th CIRP Conf. on Model. of Mach. Oper., Sintra, Portugal. Publ. in Adv. Mater. Res. 223 (2011) 75–84.
[39] C. Spaans, The mechanics of oblique cutting, taking into account the forces on the clearance face, Int. J. Mach. Tool Des. Res. 10/2 (1970) 213–220.
[40] E. J. A. Armarego, The unified-generalised mechanics of cutting approach - a step towards a house of predictive performance models for machining operations, Proc. of the 3rd CIRP Int. Workshop on Model. of Mach. Oper., Sydney, Australia (2000) 6–24.
[41] S. Campocasso, J. P. Costes, G. Fromentin, S. Bissey-Breton, G. Poulachon, Improvement of cutting forces modeling based on oriented cutting tests, Proc. of the 14th CIRP Conf. on Model. of Mach. Oper., Turin, Italy. Publ. in Procedia CIRP 8 (2013) 206–211.
[42] J. Denavit, R. S. Hartenberg, A kinematic notation for lower-pair mechanisms based on matrices, J. Appl. Mech. 22/2 (1955) 215–221.
[43] R.-S. Lee, C.-H. She, Developing a postprocessor for three types of five-axis machine tools, Int. J. Adv. Manuf. Technol. 13/9 (1997) 658–665.
[44] J. F. Hsieh, P. D. Lin, Mathematical model of multiflute drill point, Int. J. Mach. Tools Manuf. 42/10 (2002) 1181–1193.
[45] K. Sambhav, A. Kumar, S. K. Choudhury, Mechanistic force modeling of single point cutting tool in terms of grinding angles, Int. J. Mach. Tools Manuf. 51/10–11 (2011) 775–786.
[46] S. Han-Min, A new method for analysing and calculating angles on cutting tools, Int. J. Mach. Tool Des. Res. 22/3 (1982) 177–196.
[47] Sandvik Coromant, Modern Metal Cutting, 1994.
[48] S. Tomažic, S. Stančin, Simultaneous orthogonal rotations angle, Elektrotehniški Vestnik 78/1–2 (2011) 7–11.
[49] ISO, Indexable inserts for cutting tools - designation, ISO 1832, 2012.
[50] J. C. Outeiro, V. P. Astakhov, The role of the relative tool sharpness in modelling of the cutting process, Proc. of the 8th CIRP Int. Workshop on Model. of Mach. Oper., Chemnitz, Germany (2005) 517–523.
[51] B. Storch, A. Zawada-Tomkiewicz, Distribution of unit forces on the tool nose rounding in the case of constrained turning, Int. J. Mach. Tools Manuf. 57 (2012) 1–9.
[52] E. J. A. Armarego, R. H. Brown, The Machining of Metals, Prentice Hall, 1969.
[53] E. J. A. Armarego, P. Samaranayake, Performance prediction models for turning with rounded corner plane faced lathe tools. i. theoretical development, Mach. Sci. Technol. 3/2 (1999) 143–172.
[54] F. Atabey, I. Lazoglu, Y. Altintas, Mechanics of boring processes - part i, Int. J. Mach. Tools Manuf. 43/5 (2003) 463–476.
[55] T. Moriwaki, K. Okuda, Machinability of copper in ultra-precision micro diamond cutting, CIRP Ann. - Manuf. Technol. 38/1 (1989) 115–118.
[56] W. Grzesik, Stereometric and kinematic problems occurring during cutting with single-edged tools, Int. J. Mach. Tool Des. Res. 26/4 (1986) 443–458.
[57] R. Komanduri, M. Lee, L. M. Raff, The significance of normal rake in oblique machining, Int. J. Mach. Tools Manuf. 44/10 (2004) 1115–1124.
[58] J. F. Hsieh, Mathematical modeling of interrelationships among cutting angles, setting angles and working angles of single-point cutting tools, Appl. Math. Model. 34/10 (2010) 2738–2748.